MTM1 overexpression prevents and reverts BIN1-related centronuclear myopathy

Quentin Giraud, Coralie Spiegelhalter, Nadia Messaddeq, Jocelyn Laporte

BRAIN
ORIGINAL ARTICLE

MTM1 overexpression prevents and reverts BIN1-related centronuclear myopathy

Quentin Giraud, Coralie Spiegelhalter, Nadia Messaddeq and Jocelyn Laporte

See Asgarian *et al*. (https://doi.org/10.1093/brain/awad310) for a scientific commentary on this article.

Centronuclear and myotubular myopathies (CNM) are rare and severe genetic diseases associated with muscle weakness and atrophy as well as intracellular disorganization of myofibres. The main mutated proteins control lipid and membrane dynamics and are the lipid phosphatase myotubularin (MTM1), and the membrane remodelling proteins amphiphysin 2 (BIN1) and dynamin 2 (DNM2). There is no available therapy. Here, to validate a novel therapeutic strategy for BIN1- and DNM2-CNM, we evaluated adeno-associated virus-mediated MTM1 (AAV-MTM1) overexpression in relevant mouse models.

Early systemic MTM1 overexpression prevented the development of the CNM pathology in *Bin1*$^{mck-/-}$ mice, while late intramuscular MTM1 expression partially reverted the established phenotypes after only 4 weeks of treatment. However, AAV-MTM1 injection did not change the *DNM2*-CNM mouse phenotypes. We investigated the mechanism of the rescue of the myopathy in BIN1-CNM and found that the lipid phosphatase activity of MTM1 was essential for the rescue of muscle atrophy and myofibre hypotrophy but dispensable for the rescue of myofibre disorganization including organelle mis-position and T-tubule defects. Furthermore, the improvement of T-tubule organization correlated with normalization of key regulators of T-tubule morphogenesis, dysferlin and caveolin.

Overall, these data support the inclusion of *BIN1*-CNM patients in an AAV-MTM1 clinical trial.

Institut de Génétique et de Biologie Moléculaire et Cellulaire (IGBMC), CNRS UMR7104, INSERM U1258, Université de Strasbourg, 67404, Illkirch, France

Correspondence to: J. Laporte
Institut de Génétique et de Biologie Moléculaire et Cellulaire
67404 Illkirch, France
E-mail: jocelyn@igbmc.fr

Keywords: congenital myopathy; neuromuscular disease; skeletal muscle; gene therapy; mTOR

Introduction

Centronuclear and myotubular myopathies (CNM) are rare genetic diseases associated with muscle weakness and atrophy.[1] There is no current therapy for these severe diseases. Severity ranges from neonatal hypotonia to adult-onset, with non-progressive or slightly progressive development, and often correlates with respiratory distress. Histopathological hallmarks in muscle biopsies include myofibre hypotrophy, alteration of sarcomere organization, and mispositioning of nuclei and mitochondria.[2] CNM are caused by mutations mainly in the *MTM1*, *BIN1*, *DNM2*, *RYR1* or *SPEG* genes that encode proteins implicated in membrane remodelling and trafficking and excitation-contraction coupling.[3,4] In particular, *MTM1* encodes the phosphoinositides phosphatase myotubularin, *BIN1* codes for the membrane remodelling protein amphiphysin 2, and *DNM2* for dynamin 2, a mechanoenzyme fissioning membrane.[5-8] Membrane remodelling is key for the formation and maintenance of triads, endocytosis and intracellular protein transport, all important for muscle contraction and muscle hypertrophy.[9-11] Of note, BIN1 binds both MTM1 and DNM2.[12-15] As BIN1 and DNM2 were shown to be implicated in T-tubule biogenesis and maintenance, and as MTM1 regulates membrane trafficking, we hypothesize that these three proteins could be part of the same cellular pathway.[15-17]

Received December 23, 2022. Revised June 30, 2023. Accepted July 06, 2023. Advance access publication July 25, 2023

Relevant mouse models were developed and include *Mtm1*$^{-/y}$, *Bin1*$^{mck-/-}$ and *Dnm2*$^{S619L/+}$.[18-20] They were instrumental to validate the first therapeutic proofs-of-concept. Adeno-associated virus (AAV) encoding *MTM1* was previously successfully used as a gene replacement strategy for both mouse and dog models of the X-linked *MTM1*-CNM.[21] In mice, such effect was partly dependent on the phosphatase activity of MTM1, as the phosphatase-dead mutant C375S rescued the muscle atrophy, force and histopathology while fibre hypotrophy and triad shape were only partially ameliorated.[22] However, it was never reported if MTM1 modulation could rescue other genetic CNM forms.

Here we aimed to assess the efficacy of MTM1 overexpression to rescue the autosomal *BIN1*- and *DNM2*-CNM forms.

Materials and methods

Animals

Mice were placed in ventilated cages with free access to food and water in temperature-controlled rooms with 12 h daylight/dark cycles. The *Bin1*$^{mck-/-}$ mouse line was established by crossing mice floxed for exon 20 (*Bin1*$^{fl/fl}$)[23] with *Bin1*$^{fl/+}$ mice expressing the Cre recombinase under the control of MCK-Cre (The Jackson Laboratory).[24] Both lines were on a pure C57BL/6J background. Finger biopsies were used for genotyping testing for the floxed allele with 5′-AGTGAC CTAGGACTGTACCCAGAG-3′ and 5′-ACAGGTAG GTGAAAGAGACT TGG-3′ and the Cre recombinase gene with 5′-GAACCTGATGGACA TGTTCAGG-3′ and 5′-AGTGCGTTCGAACGCTAGAGCCTGT-3′. The *Dnm2*$^{S619L/+}$ mutant mouse line was created at the Institut Clinique de la Souris (http://www.ics-mci.fr/en/).[20] The following primers were used for genotyping: E forward (Ef): 5′-CAGAAAGCAGGATCCT CGGTGCC-3′; E reverse (Er): 5′-AGTCCAGCTCTGGCTTTGGATCGC-3′; for sequencing: Mf: 5′-CCAGAGCCCATGGTCTTAGTGGCC-3′; Mr: 5′-ACCCCAGCGCGCAGGAACAG-3′. Male littermates were sacrificed at 10 or 12 weeks of age for the *Bin1*$^{mck-/-}$ line while males and females were used for the *Dnm2*$^{S619L/+}$ mutant line and sacrificed at 8 weeks. A total of 166 mice were used in this study. Male pups from the *Bin1*$^{mck-/-}$ line were randomly injected at birth with the treatment or the control before assessment of their genotype. When possible, half of the litter was injected with the treatment and the other with the control. Male siblings were housed together independently of their genotype or treatment. Owing to the observed reduced viability of the *Dnm2*$^{S619L/+}$ pups, which caused unequal group size, the male and female pups from the *Dnm2*$^{S619L/+}$ line were genotyped and then treated accordingly. Females were housed independently of treatment or genotype as well as male siblings. Pups from both lines were injected intraperitoneally with 50 µl of AAV solution at 9.8×10^{12} genome copies per ml. Six-week-old males from the *Bin1*$^{mck-/-}$ line were injected intramuscularly in tibialis anterior (TA) muscle with 20 µl of AAV solutions at 7×10^{11} genome copies per ml. Group sizes were established on the basis of previous studies on the same line of mice.[19,20] No exclusion criteria were used. All cages were housed in the same room and placed in random order on the rack. The injections were administered by a single experimenter (Q.G.), who was blinded to the genotype of male pups from the *Bin1*$^{mck-/-}$ line but aware of the genotype for adult males and *Dnm2*$^{S619L/+}$ pups. The assignment of treatment for a given genotype was randomized.

Antibodies

Myotubularin antibody [made in-house, #2827, rabbit polyclonal against MTM_PI168 peptide (QMMPHVQTH)] was used in western blot, diluted 1/1000. Dynamin-2 antibody [made in-house, #2865, rabbit polyclonal against PRD domain (HSPTPQRRPVSSVHPP GRPPAVR)] was used in western blot, diluted 1/700. Caveolin-3 antibody (Santa Cruz, sc-5310) was used in western blot, diluted 1/200. Dysferlin antibody (Abcam, ab124684) was used in western blot, diluted 1/1000. Akt antibody (Cell Signaling Technology, #9272) was used in western blot, diluted 1/1000. Phospho-Akt antibody (Ser473) (Cell Signaling Technology, #9271) was used in western blot, diluted 1/2000. S6 Ribosomal Protein antibody (Cell Signaling Technology, #2217) was used in western blot, diluted 1/1000. Phospho-S6 Ribosomal Protein antibody (Ser235/236) (Cell Signaling Technology, #2211) was used in western blot, diluted 1/1000. Peroxidase AffiniPure F(ab′)$_2$ Fragment Goat Anti-Rabbit IgG (H + L) antibody (Jackson ImmunoResearch, 111-036-045) was used in western blot, diluted 1/10 000. Peroxidase AffiniPure F(ab′)$_2$ Fragment Goat Anti-Mouse IgG + IgM (H + L) (Jackson ImmunoResearch, 111-036-045) used in western blot, diluted 1/10 000. Myosin heavy chain Type IIA antibody (SC-71 deposited to the DSHB by Schiaffino S.) was used for immunofluorescence at 1/50 dilution. Myosin heavy chain type I antibody (BA-D5 deposited to the DSHB by Schiaffino S.) was used for immunofluorescence at 1/50 dilution. Myosin heavy chain Type IIB antibody (BF-F3 deposited to the DSHB by Schiaffino S.) was used for immunofluorescence at 1/50 dilution. Cy3 AffiniPure Goat Anti-Mouse IgG, Fcγ subclass 2b specific antibody (Jackson ImmunoResearch, 115-165-207) was used for immunofluorescence at 1/100 dilution. Alexa Fluor 488 AffiniPure Goat Anti-Mouse IgG, Fcγ subclass 1 specific antibody (Jackson ImmunoResearch, 115-545-205) was used for immunofluorescence at 1/100 dilution. DyLight 405 AffiniPure Goat Anti-Mouse IgM, µ chain specific antibody (Jackson ImmunoResearch, 115-475-075) was used for immunofluorescence, at 1/100 dilution.

AAV construction and production

Recombinant AAVs serotype 9 were generated by triple transfection of HEK293T-derived cell line with the expression plasmid pAAV-MTM1 or pAAV-MTM1 C375S and the auxiliary plasmids pHelper (Agilent) and pAAV2/9 P0008 (Penn Vector Core). Murine MTM1 wild-type and phosphatase dead cDNA were cloned under the control of CMV promoter in the pAAV-MCS (Agilent) plasmid. Recombinant AAVs (rAAV) were harvested 48 h after transfection from cell lysate treated with 100 U/ml Benzonase (Merck). AAV9 were purified by Iodixanol gradient ultracentrifugation (OptiprepTM, Axis Shield) followed by dialysis and concentration against Dulbecco's PBS containing 0.5 mM $MgCl_2$ using centrifugal filters (Amicon Ultra-15 Centrifugal Filter Device 100 K). Viral titres were determined by qPCR using the LightCycler480 SYBR Green I Master (Roche) and primers targeting the CMV enhancer sequence. Viruses were stored at −80°C until use.

Motor tests

From 3 weeks of age, systemically injected mice were phenotyped once per week until 10 or 12 weeks of age for the *Dnm2*$^{S619L/+}$ mutant line and *Bin1*$^{mck-/-}$ line, respectively. Body weight and whole-body hanging ability were measured. The hanging test was performed by suspending the mice in a cage lid and then turned upside-down for up to 60 s, and the time to fall was recorded. This experiment was repeated three times per mouse per week, with a 15 s interval to measure fatiguability. At 10 or 12 weeks of

age, the mice were housed overnight in an actimeter (imetronic) and their motor activity was measured from 18:42 to 8:22.

From 6 weeks of age, intramuscularly-injected mice were submitted to weekly leg strength measurement with the Complete1300A mouse Test System (Aurora Scientific). Mice were anaesthetized with 1–2% isoflurane and the leg was fixed to the footplate; the TA muscle was directly stimulated at 20 mA and 100 Hz to measure maximal force. The specific maximal force was obtained by dividing the absolute muscle force by the mouse weight at the time of the test. All tests were performed by the same experimenter (Q.G.) who was aware of the group allocation at all stages except when performing the hanging test. Mice were phenotyped in random order.

Muscle contractile properties

TA muscle contraction properties were evaluated by measuring in situ muscle contraction after sciatic nerve stimulation using the Complete1300A mouse Test System (Aurora Scientific). Mice were anaesthetized by sequential intraperitoneal injections of Domitor/Fentadon mix (2 and 0.28 mg/kg), diazepam (8 mg/kg) and fentanyl (0.28 mg/kg). Afterward, TA distal tendon was detached and tied to an isometric transducer. The sciatic nerve was then stimulated by pulses of 1–125 Hz of 8 mA, and the absolute maximal force was determined. The specific maximal force was obtained by dividing the absolute muscle force by the TA cross-sectional area determined by dividing the muscle mass (in mg) by the product of the optimal muscle length (in mm) and the density of mammalian skeletal muscle (1.06 mg/mm^3).

Sample collection and histology

TA, quadriceps and soleus muscles were dissected and weighted. Muscles were then frozen in liquid nitrogen-cooled isopentane and stored at –80°C for haematoxylin and eosin and succinate dehydrogenase (SDH) histology analysis. Blood was collected in heparin-coated tubes and plasma was stored at –80°C. Heart, diaphragm and liver were snap-frozen in liquid nitrogen. Transversal cryosections (8 µm) were prepared and stained and were observed using the Hamamatsu 322 NanoZoomer 2HT slide-scanner. Myofibre size was measured by the Cellpose segmentation algorithm on haematoxylin and eosin sections.[25] Classification of the myofibres presenting abnormal SDH staining was done manually with Fiji and QuPath software.[26,27]

Enzyme assay

Plasma samples were analysed using an AU480 Chemistry Analyzer (Beckman Coulter). As per the manufacturer's recommendation, haemolysed samples were excluded from measurements of aspartate aminotransferase and total bilirubin.

Electron microscopy

The samples were fixed by immersion in 2.5% glutaraldehyde and 2.5% paraformaldehyde in cacodylate buffer (0.1 M, pH 7.4), and washed in cacodylate buffer for further 30 min. The samples were postfixed in 1% osmium tetroxide in 0.1 M cacodylate buffer for 1 h at 4°C and dehydrated through graded alcohol (50, 70, 90 and 100%) and propylene oxide for 30 min each. Samples were oriented and embedded in Epon 812. Semithin sections were cut at 2 µm and ultrathin sections were cut at 70 nm (Leica Ultracut UCT) and contrasted with uranyl acetate and lead citrate and examined at 70 kV with a Morgagni 268D electron microscope (FEI Electron Optics) equipped with a Mega View III camera (Soft Imaging System) or with a Philips CM12 electron microscope equipped with a Gatan OneView Camera (Gatan).

Western blotting

TA muscle cryosections were lysed overnight in RIPA buffer supplemented with 1 mM PMSF, 1 mM sodium orthovanadate, 5 mM sodium fluoride and cOmplete mini-EDTA free protease inhibitor cocktail (Roche Diagnostics Cat. No. 11 836 170 001). Protein concentrations were calculated using a DC Protein Assay Kit (Bio-Rad #5000116). Protein (10 µg) in 4× Lane Marker Reducing Buffer (Thermo Fisher Scientific #39000) were separated in 10% SDS-PAGE gel made with TGX Stain-Free FastCast Acrylamide Kit, 10% (Bio-Rad 1610183). PageRuler™ Plus Prestained Protein Ladder (Thermo Fisher Scientific #26620) (8 µl) was run alongside for reference. The gel was transferred on nitrocellulose membrane (Bio-Rad 170427) using a Transblot Turbo RTA transfer kit (Bio-Rad 1704271) for 10 min at 2.5 A. Normalization of protein loading was determined by Ponceau S staining. Membranes were blocked for 1 h in TBS containing 5% non-fat dry milk and 0.1% Tween-20 (Merck P2287-500 Ml) before a 1-h room temperature or overnight 4°C incubation with a given primary antibody. Subsequently, membranes were incubated with secondary antibodies coupled to horseradish peroxidase (Jackson ImmunoResearch). Membrane stripping was done by 45-min incubation with agitation in Western ReProbe™ PLUS (G-Biosciences #786-307) then washed three times with TBS-T.

Nitrocellulose membranes were visualized in Amersham Imager 600 (GE Healthcare Life Sciences) after the addition of SuperSignal West Pico PLUS chemiluminescent Substrate (Thermo Fisher #34579). The Fiji software was used for the quantification of the band intensity in the images.

Phosphatidylinositol 3-phosphate mass ELISA

Phosphatidylinositol lipids were extracted from frozen gastrocnemius muscles grounded in liquid nitrogen. The frozen muscle powder was suspended in 3 ml of 5% trichloroacetic acid and 1 mM EDTA ice-cold solution, agitated for 30 s then centrifuged at 3000 rpm for 5 min at 4°C. The supernatant was then discarded and the washing step repeated once. The pellet was resuspended in 3 ml of MeOH:$CHCl_3$ (2:1) solution under agitation for 10 min and then centrifugated at 3000 rpm for 5 min at room temperature. The supernatant was then discarded and the wash repeated once. The remaining pellet was then resuspended in 2.25 ml of MeOH:$CHCl_3$:12 N HCl (80:40:1) under agitation for 25 min. This solution was then centrifugated at 3000 rpm for 5 min, the supernatant was then collected and mixed with 0.75 ml of $CHCl_3$ and 1.35 ml of 0.1 N HCl. After 30 s of agitation the solution was centrifugated at 3000 rpm for 5 min and the lower phase was then collected and dried in a vacuum dryer until complete evaporation.

The remaining lipids were then quantified by mass ELISA in a single experiment using three commercial kits (Echelon Bioscience Inc #K-3300). The absorbance at 450 nm was measured with a plate reader (BioTek, Synergy HTX Multimode Reader). The corresponding Ptdlns3P values were inferred from the standard curve using a non-linear regression analysis with GraphPad Prism software (four-parameter logistic, 4PL). Absorbance values between 0 and 0.39 pmol were extrapolated from the standard curve. The

raw Ptdlns3P values were then normalized to the corresponding muscle weight.

RNA and DNA extraction

Frozen tissues samples were mechanically lysed with a Precellys homogenizer (Bertin technologies) in TRIzol reagent (Thermo Fisher #15596026) and processed according to the manufacturer's instructions to obtain total RNA. Genomic and vector DNA were extracted using the Puregene Tissue Kit (Qiagen #158063).

Quantitative real-time PCR

The murine titin (*Ttn*) gene was used for the standardization of transgene copies per diploid genome. 5′-TTC AGT CAT GCT GCT AGC GC-3′ (forward), 5′-AAA ACG AGC AGT GAC GTG AGC-3′ (reverse). Amplification of the *Mtm1* transgene was done using a primer pair matching exon 10 and 11. 5′-TTG GTT GTC CAG TTT GGA GTC TAC T-3′ (forward), 5′-CCG TCA CTG CAA TGC ACA AG-3′ (reverse). For quantification of transgene expression, cDNA was produced from RNA extract using SuperScript IV Reverse Transcriptase (Thermo Fisher #18090010) according to the manufacturer's instruction. The *Rps11* gene was used for standardization 5′-CGC GTG GTG AAT AAG GAA GC-3′ (forward), 5′-GTA AGC ACG CTC CGT CTG AA-3′ (reverse). Endogenous *Mtm1* expression was quantified using a primer pair matching exon 14 and 15. 5′-ATC CGA TGG AAT CCC AGG GT-3′ (forward), 5′-CCA TCT GTG ACG AAC TGG AA-3′ (reverse). Exogenous *Mtm1* expression was quantified using a reverse primer matching a silent GAG tag present in the transgene sequence 5′-CCA TCT GTG ACG AAC TGC TC-3′ (reverse). Reactions were prepared with SYBR Green Master Mix I (Roche # 04707516001) and run in a lightcycler 480 (Roche). qRT-PCR was performed using technical replicates.

Immunofluorescence

Cryosections (8-μm thick) of TA were incubated for 1 h with 3% bovine serum albumin (BSA) in PBS and then washed three times with PBS. Cryosections were incubated with primary antibodies in PBS 3% BSA overnight or with only PBS 3% BSA for negative controls, then washed three times. Secondary antibodies were incubated for 1 h at room temperature then cryosections were washed three times with PBS then mounted with FluorSave™ Reagent (Merck #345789) and kept at 4°C until analysis.

Statistics

All data were verified for normal or log-normal distribution using D'Agostino and Pearson test if the sample size was superior to seven, otherwise Shapiro-Wilk test was used. If all groups fitted the log-normal distribution, all groups were log-transformed for subsequent statistical analysis. If normality was confirmed, one-way ANOVA was used, if technical replicates were available then nested one-way ANOVA was used instead. Homoscedasticity was then assessed with the Brown-Forsythe and Bartlett's test and heteroscedastic data were analysed with Brown-Forsythe and Welch ANOVA tests instead of ordinary ANOVA. If one or several groups did not fit a normal or log-normal distribution, they were analysed with non-parametric tests. Multiple comparisons of normal homoscedastic and heteroscedastic data were done by Fisher's LSD test and by unpaired *t*-test with Welch's correction, respectively. For non-normally distributed data, uncorrected Dunn's test was used. When comparing two samples from the same animal, paired comparisons were used. The force ratio between contralateral legs was evaluated against a hypothetical mean of 1 by one-sample *t*-test. A *P*-value < 0.05 was considered significant. All statistical tests used were two-sided. Multiple time points were analysed separately. Charts show individual points with additional lines indicating mean ± standard error of the mean (SEM). Curves and graphs were made using GraphPad Prism 9 software.

Study approval

Animal care and experimentation were in accordance with French and European legislation and approved by the institutional ethics committee (project numbers APAFIS#22713-2019103108289018 and APAFIS#31976-202106111155641).

Results

Systemic MTM1 overexpression does not rescue the DNM2-CNM mouse

First, we tested if MTM1 overexpression can rescue the motor and histopathological phenotypes of the *Dnm2*$^{S619L/+}$ mouse (named 'SL' in figures), a relevant model harbouring the most frequent mutation in severe cases of *DNM2*-CNM.[20,28] These mice display impaired motor function apparent at 3 weeks, decreased muscle force, myofibre hypotrophy and mitochondria misposition. Systemic MTM1 overexpression was achieved through intraperitoneal injection at P1 of AAV carrying the murine *Mtm1* cDNA coding for the full-length wild-type protein (AAV-MTM1-WT). Treated males and females were analysed from 3 to 8 weeks and compared to AAV-empty injected littermates. AAV-MTM1-WT did not improve motor function in hanging tests and spontaneous activity, nor body weight (Fig. 1A–C). The muscle atrophy was not improved in different muscles (Fig. 1D and Supplementary Fig. 1A) and the weaker specific maximal force of isolated muscle was not changed (Fig. 1E and Supplementary Fig. 1B and C). AAV-MTM1-WT did not rescue the typical CNM histopathology and myofibres remained smaller with a central accumulation of mitochondria revealed by SDH oxidative stain (Fig. 1F and G, Supplementary Fig. 1D and E). Muscles of *Dnm2*$^{S619L/+}$ mice injected with AAV-MTM1-WT overexpressed MTM1 to about 16-fold compared to endogenous level, while the higher DNM2 protein level due to the S619L mutation was not decreased toward wild-type level with the treatment (Supplementary Fig. 1F and G). Overall, these data showed that early systemic increase of MTM1 did not ameliorate any signs of CNM in the *Dnm2*$^{S619L/+}$ mouse.

Systemic MTM1 overexpression strongly improves muscle function and force of the BIN1-CNM mouse

We next evaluated the potential of MTM1 overexpression to rescue the *BIN1*-CNM form using a similar protocol, intraperitoneal injection of AAV at P1 to drive systemic expression of MTM1-WT in the *Bin1*$^{mck-/-}$ mouse lacking BIN1 specifically in muscle (named 'KO' in figures). *Bin1*$^{mck-/-}$ mouse displays muscle force deficit and histopathology typical of CNM, apart from the centralized nuclei, while constitutive *Bin1* deletion is lethal at birth precluding the testing of rescuing strategies for disease prevention or reversion.[19] While *Bin1*$^{mck-/-}$ mice displayed decreased hanging time starting from 6 weeks and decreased spontaneous activity (rears and distance travelled) at 10 weeks, AAV-MTM1-WT normalized motor function at all ages (Fig. 2A and B and Supplementary Fig. 2A). At 10 weeks, quadriceps and TA muscle atrophy was improved upon

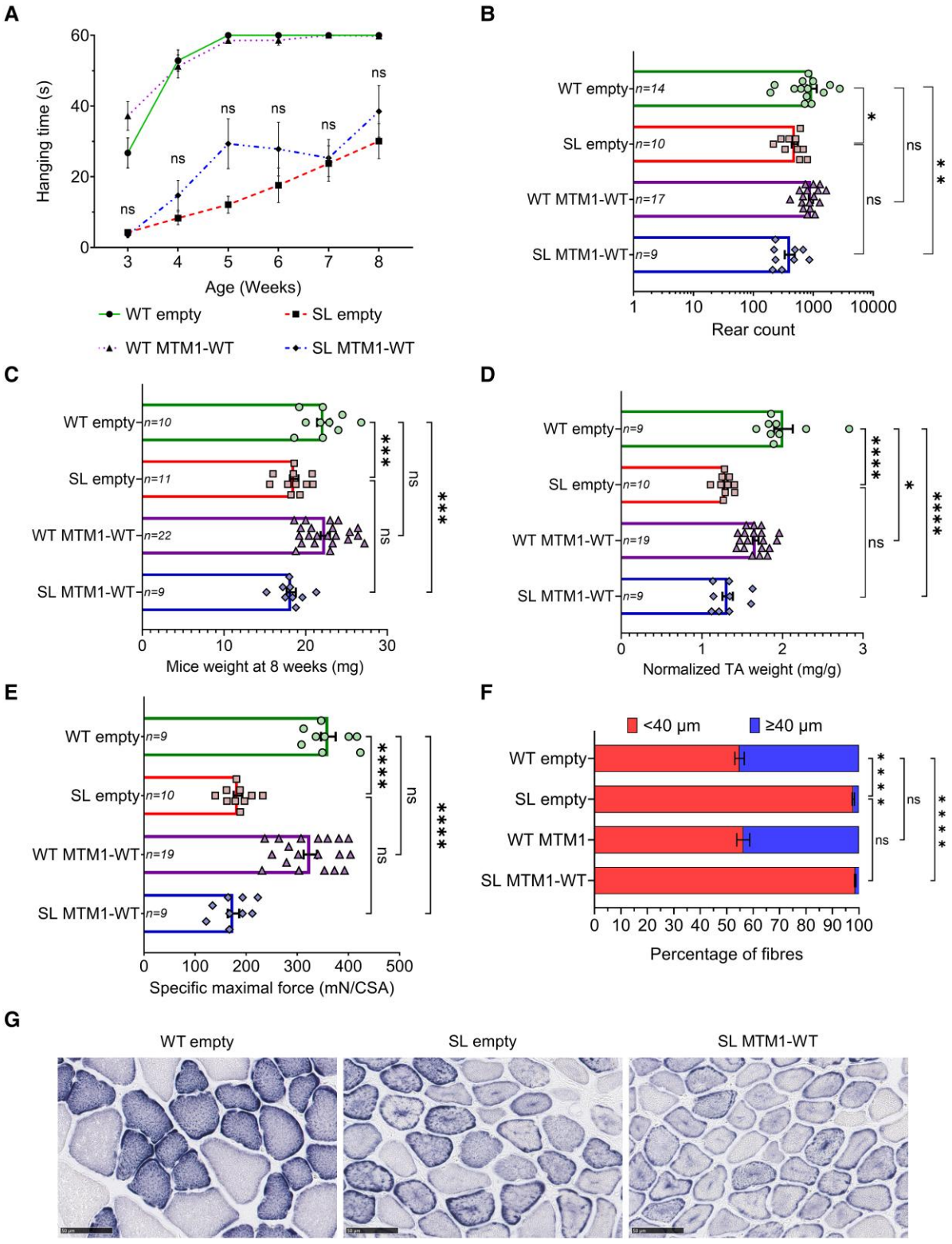

Figure 1 Systemic MTM1 overexpression does not improve the hallmarks of the *Dnm2*$^{S619L/+}$ mouse model of centronuclear and myotubular myopathies (CNM). (**A**) Hanging test performance, maximum hanging time is 60 s ($n \geq 9$; unpaired *t*-test between SL empty and SL MTM1-WT group at each time point). (**B**) Spontaneous activity (rears on hindlimbs) measured overnight at 8 weeks of age in actimetry cages ($n \geq 9$). (**C**) Body weight at 8 weeks of age ($n \geq 9$). (**D**) Tibialis anterior (TA) muscle weight normalized to body weight ($n \geq 9$). (**E**) Specific maximal muscle force measured *in situ* in response to stimulation of 100 Hz ($n \geq 9$). (**F**) Repartition between large (≥40 µm) and small (<40 µm) fibres (MinFeret diameter, $n = 5$). (**G**) Representative images of TA stained for succinate dehydrogenase (SDH) from 8-week-old animals. Scale bar = 50 µm. Kruskal-Wallis test followed by Dunn's test, one-way ANOVA followed by Fisher's LSD test, unpaired *t*-test with Welch's correction, $^{*}P < 0.05$, $^{**}P < 0.01$, $^{***}P < 0.001$, $^{****}P < 0.0001$. SL = *Dnm2*$^{S619L/+}$ mouse; ns = not significant; WT = wild-type.

treatment (Fig. 2C and D). We verified that the MTM1 protein was overexpressed in the muscle of AAV-MTM1-WT injected mice (Supplementary Fig. 2C). The specific maximal force and submaximal forces (force-frequency) were fully normalized in *Bin1*$^{mck-/-}$ mice with AAV-MTM1-WT while muscle force remained strongly impaired at all stimulation frequencies with AAV-empty (Fig. 2E and F). Muscle contraction upon repeated stimulations at submaximal force frequency was abnormal in *Bin1*$^{mck-/-}$ mice, while it was similar to wild-type mice upon AAV-MTM1-WT injection (Fig. 2G). These data showed that MTM1-WT exogenous expression normalized the strong motor defect and force deficit of the *BIN1*-CNM mouse.

MTM1 overexpression improves myofibre organization in the BIN1-CNM mouse

To investigate the basis of the normalized muscle function upon MTM1-WT expression in the *Bin1*$^{mck-/-}$ mice, histological and ultrastructural analyses were performed. At 10 weeks, myofibre hypotrophy of the *Bin1*$^{mck-/-}$ mice was significantly improved with AAV-MTM1-WT (Fig. 3A–C and Supplementary Fig. 3A). The mitochondria position was fully normalized (Fig. 3D and Supplementary Fig. 3C). At the ultrastructural level, electron microscopy revealed an altered sarcomere organization in *Bin1*$^{mck-/-}$ muscle that was normalized upon MTM1-WT expression (Fig. 3E). CNM are associated with defects in the T-tubule network and BIN1 regulates T-tubule biogenesis.[3,15] Ferrocyanate labelling of T-tubules followed by electron microscopy revealed that the number of T-tubules per sarcomere and their width were also corrected upon MTM1-WT expression (Fig. 3F and G). In conclusion, MTM1-WT expression was able to normalize the muscle function of the *BIN1*-CNM mouse through the improvement of myofibre organization and T-tubule ultrastructure.

MTM1 overexpression does not induce toxicity in various organs

To evaluate the overall expression and toxicity of MTM1-WT in 10-week-old *Bin1* KO mice, we performed quantitative measurement of transgene copy number and mRNA expression. Treated mice had on average ~30 transgene copies per genome in organs of the trunk, including the liver, heart and diaphragm while the soleus and quadriceps limb muscles had approximately three copies (Supplementary Fig. 4A). Exogenous *Mtm1* RNA relative expression, however, was similar in all organs (Supplementary Fig. 4B). In the liver, overexpression of MTM1-WT did not lead to a significant elevation of liver enzymes or total bilirubin levels, suggesting the absence of hepatic dysfunction (Supplementary Fig. 4C, D and E). Histological examination of liver and diaphragm sections stained with haematoxylin and eosin revealed no significant lesions or abnormalities. Furthermore, Masson's trichrome staining of the heart apex sections showed no evidence of fibrosis, indicating the absence of cardiac fibrotic remodelling (Supplementary Fig. 5A). The assessment of heart weight also demonstrated no signs of cardiac hypertrophy, further supporting the absence of adverse effects on cardiac structure (Supplementary Fig. 4F). Overall, these results suggest that AAV-mediated MTM1 overexpression is systemic and does not induce detectable toxicity or pathological alterations.

The dead-phosphatase MTM1 mutant ameliorates muscle function and force of the BIN1-CNM mouse

Membrane remodelling and trafficking regulate organelle structure and position and modulate signalling for normal muscle physiology. Of note, MTM1 is a lipid phosphatase that may impact membrane structure and cell signalling. To decipher further the mechanism behind the rescue of BIN1-CNM by MTM1 overexpression, we assessed the importance of MTM1 phosphatase activity through the expression of the C375S dead-phosphatase mutant (AAV-MTM1-CS) and the same methodological pipeline. MTM1-CS expression partially rescued the motor function (hanging test and rear number) of *Bin1*$^{mck-/-}$ mice while the muscle atrophy of the quadriceps or TA was not rescued (Fig. 4A–D and Supplementary Fig. 6A and B). The specific maximal force and the force-frequency relationship of the isolated TA were significantly ameliorated, and the response to repeated stimulations was closer to a wild-type response in *Bin1*$^{mck-/-}$ mice with AAV-MTM1-CS (Fig. 4E–G). Compared to MTM1-WT, which normalized motor function and muscle force and improved muscle atrophy, the expression of MTM1-CS revealed an intermediate rescue for motor function and muscle force and no detectable effect on muscle atrophy. This suggests that the benefit of MTM1-CS on motor function and force is not due to a hypertrophic effect but rather to the improvement of the intrinsic properties of myofibres.

The phosphatase activity of MTM1 is required to improve myofibre size

At 10 weeks, the fibre hypotrophy of *Bin1*$^{mck-/-}$ muscle was ameliorated with AAV-MTM1-WT and not with AAV-MTM1-CS, paralleling with the differential effect observed above on muscle atrophy (Fig. 5A–D). However, both transgenes fully normalized mitochondria position (Fig. 5B and E). We confirmed the overexpression of MTM1-CS in the analysed muscles (Supplementary Fig. 8A). The level of the main MTM1 lipid substrate, phosphatidylinositol 3-monophosphate (PtdIns3P), was quantified in gastrocnemius muscle and showed a significant reduction in *Bin1*$^{mck-/-}$ animals compared to wild-type mice, potentially due to a compensatory mechanism. As expected, overexpression of MTM1-WT in *Bin1*$^{mck-/-}$ muscle significantly decreased PtdIns3P level while it was not the case with overexpression of MTM1-CS (Fig. 5F). Overall, the phosphatase activity of MTM1 is required to improve muscle atrophy and fibre size while this activity appears dispensable for the intracellular organization of myofibres and organelle positioning.

Master regulators of muscle hypertrophy are AKT and mTOR.[29] AKT phosphorylation was decreased in *Bin1*$^{mck-/-}$ muscle and ameliorated by MTM1 overexpression (Fig. 6A and Supplementary Fig. 7A). In addition, the phosphorylation of mTOR effector ribosomal protein S6 (S6RP) was strongly upregulated (7.8-fold) in *Bin1*$^{mck-/-}$ muscle, while MTM1 overexpression had no detectable impact. Thus, hypertrophic pathways are altered in the *Bin1*$^{mck-/-}$ mouse, paralleling with its muscle atrophy and fibre hypotrophy, and the AKT activation was ameliorated upon MTM1 expression.

MTM1 expression rescues T-tubule biogenesis in the BIN1-CNM mouse

To characterize further the effect of exogenous MTM1 expression on the organization of intracellular membrane structures, we focused on the morphological aspect of T-tubules. MTM1-CS expression rescued T-tubules organization and number per sarcomere, similarly to the expression of MTM1-WT, and both proteins decreased the enlarged T-tubules in *Bin1*$^{mck-/-}$ muscle (Fig. 6B–D). T-tubule biogenesis and maintenance are regulated by BIN1 and also by dysferlin (DYSF) and caveolin 3 (CAV3).[30] To better understand the rescue of T-tubule organization in *Bin1*$^{mck-/-}$ treated

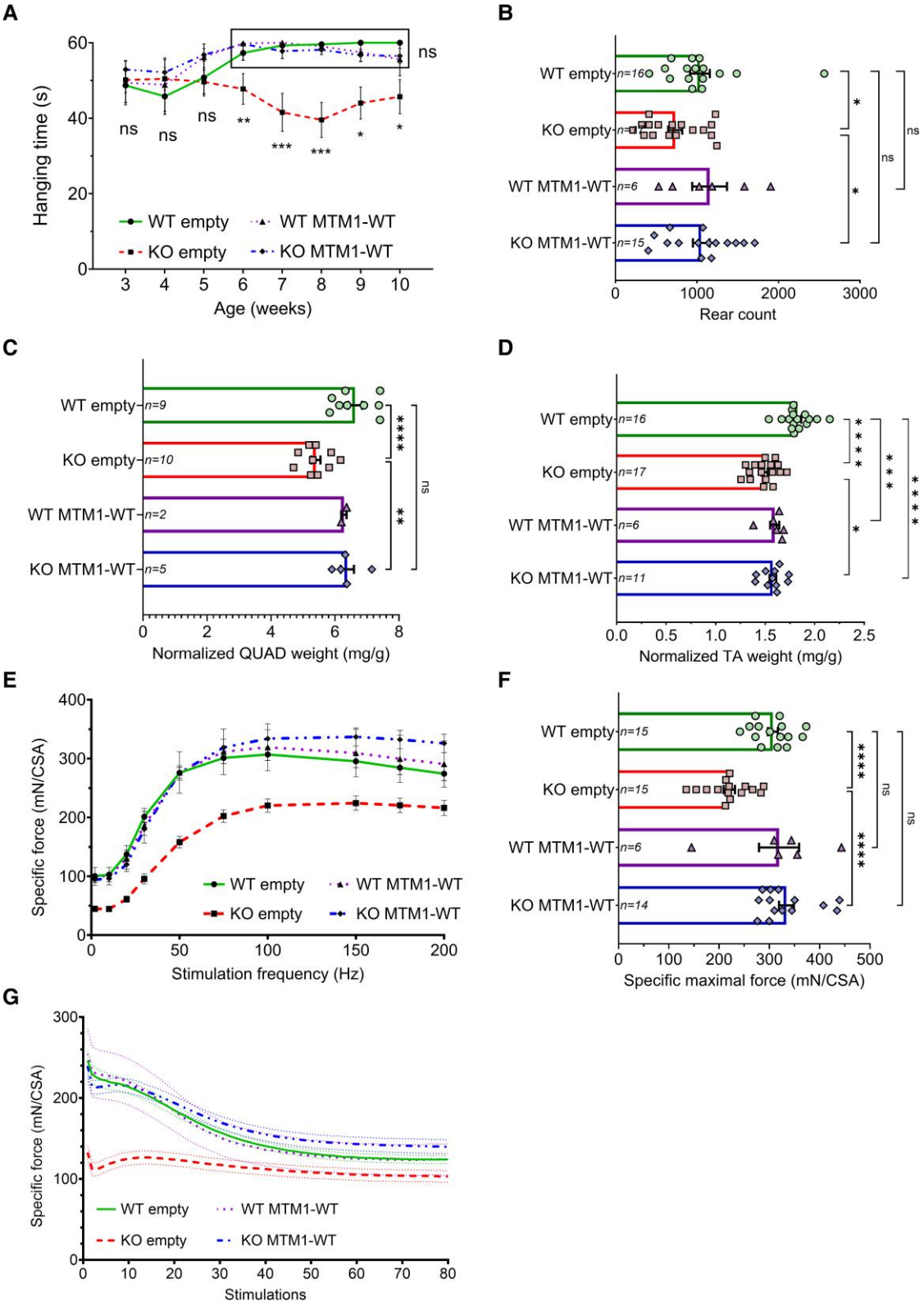

Figure 2 Systemic MTM1 overexpression normalizes motor function and muscle force of *Bin1* KO animals. (**A**) Hanging test performance, maximum hanging time is 60 s. Asterisks represent statistically significant comparisons between KO empty and KO MTM1-WT groups. The box shows groups with a non-significant (ns) difference ($n \geq 6$). (**B**) Spontaneous activity (rears on hindlimbs) measured overnight at 10 weeks of age in actimetry cages ($n \geq 6$). (**C**) Quadriceps (QUAD) muscle weight normalized by body weight ($n \geq 2$). (**D**) Tibialis anterior (TA) muscle weight normalized by body weight at 10 weeks of age ($n \geq 6$). (**E**) *In situ* specific force measurement from TA stimulated at different frequencies ($n \geq 6$). (**F**) Specific maximal muscle force measured at 100 Hz ($n \geq 6$). (**G**) Specific muscle force of the TA upon repeated stimulations at 40 Hz (1 s of stimulation and 3 s of rest, $n \geq 6$). Kruskal-Wallis test followed by Dunn's test, one-way ANOVA followed by Fisher's LSD test, nested one-way ANOVA followed by Fisher's LSD test, unpaired *t*-test with Welch's correction $^{*}P < 0.05$, $^{**}P < 0.01$, $^{***}P < 0.001$, $^{****}P < 0.0001$. KO = knockout; WT = wild-type.

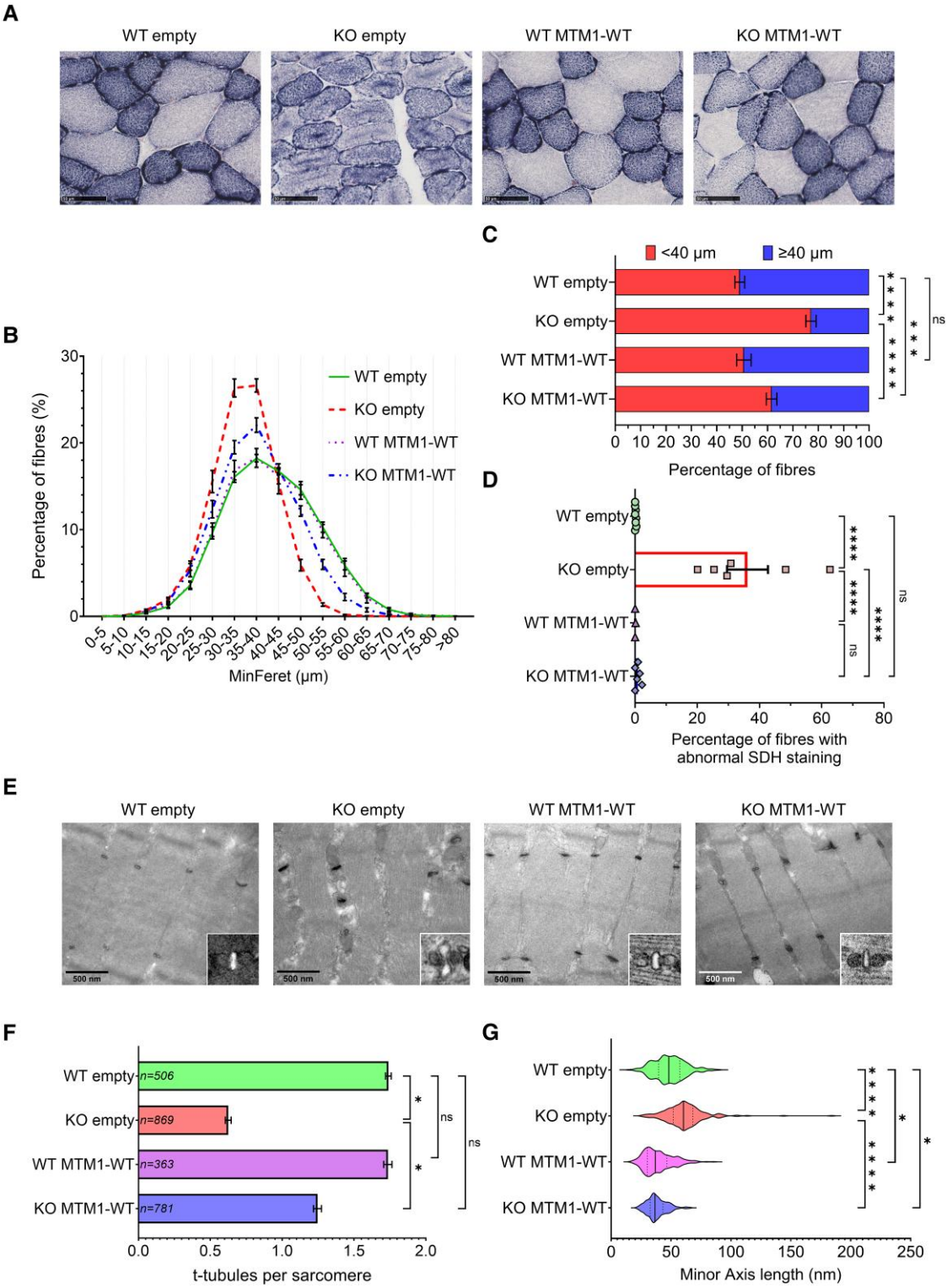

Figure 3 Systemic MTM1 overexpression improves histological hallmarks of *Bin1* KO animals. (**A**) Representative images of tibialis anterior (TA) stained by succinate dehydrogenase (SDH). Scale bar = 50 µm. (**B**) MinFeret diameter distribution of TA myofibres (**C**) and repartition between big (≥40 µm) and small (<40 µm) fibres ($n \geq 6$). (**D**) Percentage of fibres presenting SDH accumulation in their centre ($n \geq 3$). (**E**) Representative longitudinal electron microscopy pictures of TA from 10-week-old mice stained by ferrocyanate. Boxed micrographs depict electron microscopy pictures without ferrocyanate staining. Scale bar = 500 nm. (**F**) Quantification of the number of T-tubules per sarcomere ($n \geq 1$, $n \geq 209$) (**G**) and their minor axis width ($n \geq 253$). One-way ANOVA followed by Fisher's LSD test, nested one-way ANOVA followed by Fisher's LSD test, Kruskal-Wallis test followed by Dunn's test $^{*}P < 0.05$, $^{***}P < 0.001$, $^{****}P < 0.0001$. KO = knockout; WT = wild-type.

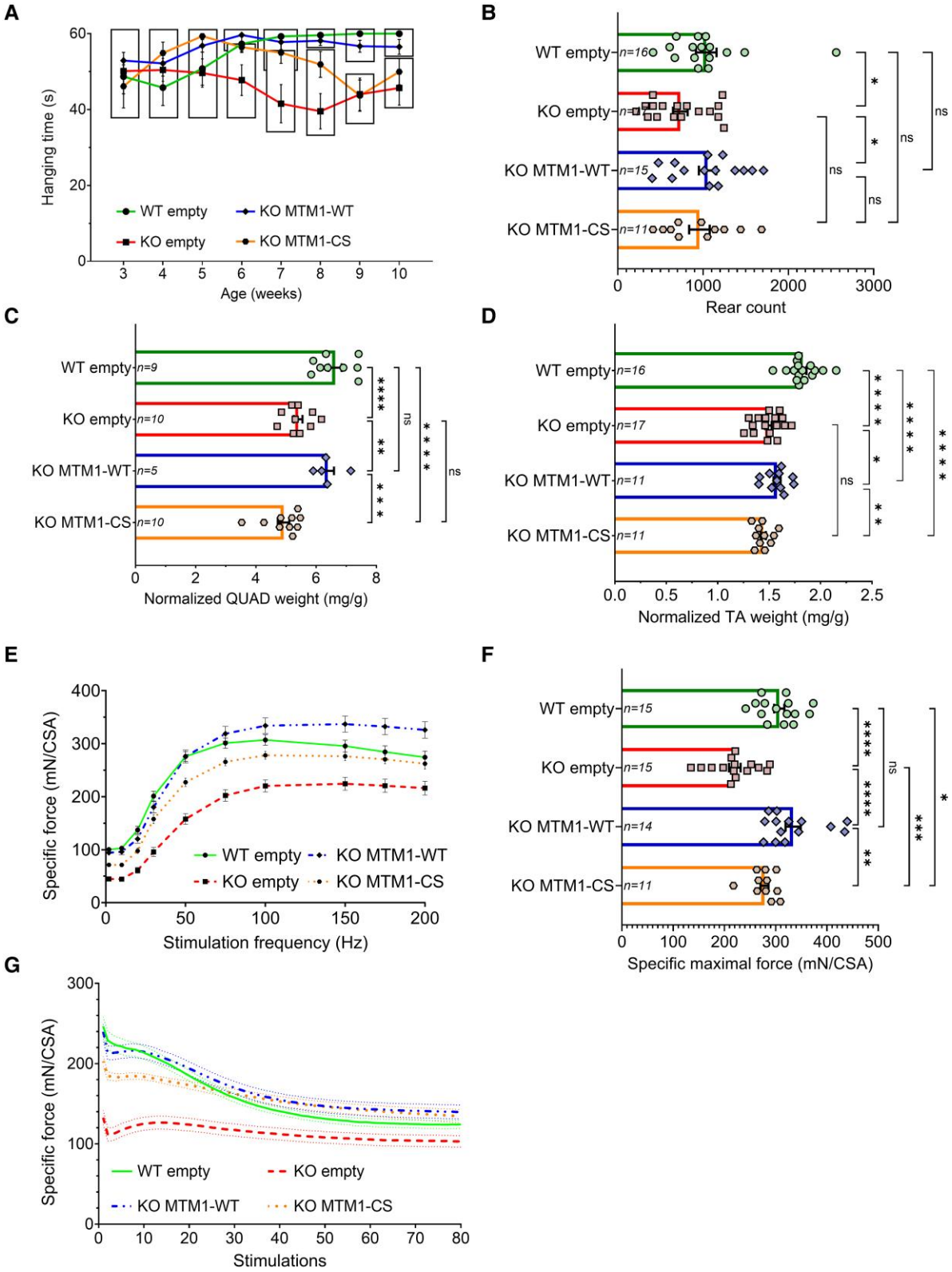

Figure 4 Systemic dead-phosphatase MTM1 overexpression partially improves motor function and muscle force of *Bin1* KO animals. (**A**) Hanging test performance, maximum hanging time is 60 s. The boxes show groups with a non-significant (ns) difference ($n \geq 11$). (**B**) Spontaneous activity (rears on hindlimbs) measured overnight at 10 weeks of age in actimetry cages ($n \geq 11$). (**C**) Quadriceps (QUAD) muscle weight normalized to body weight ($n \geq 5$). (**D**) Tibialis anterior (TA) muscle weight normalized to body weight at 10 weeks of age ($n \geq 11$). (**E**) *In situ* specific force measurement from TA stimulated at different frequencies, and (**F**) specific maximal muscle force measured at 100 Hz ($n \geq 11$). (**G**) Specific muscle force of the TA upon repeated stimulations at 40 Hz (1 s of stimulation and 3 s of rest, $n \geq 10$). Kruskal-Wallis test followed by Dunn's test, one-way ANOVA followed by Fisher's LSD test, nested one-way ANOVA followed by Fisher's LSD test, unpaired *t*-test with Welch's correction, $^{*}P < 0.05$, $^{**}P < 0.01$, $^{***}P < 0.001$, $^{****}P < 0.0001$. KO = knockout; WT = wild-type.

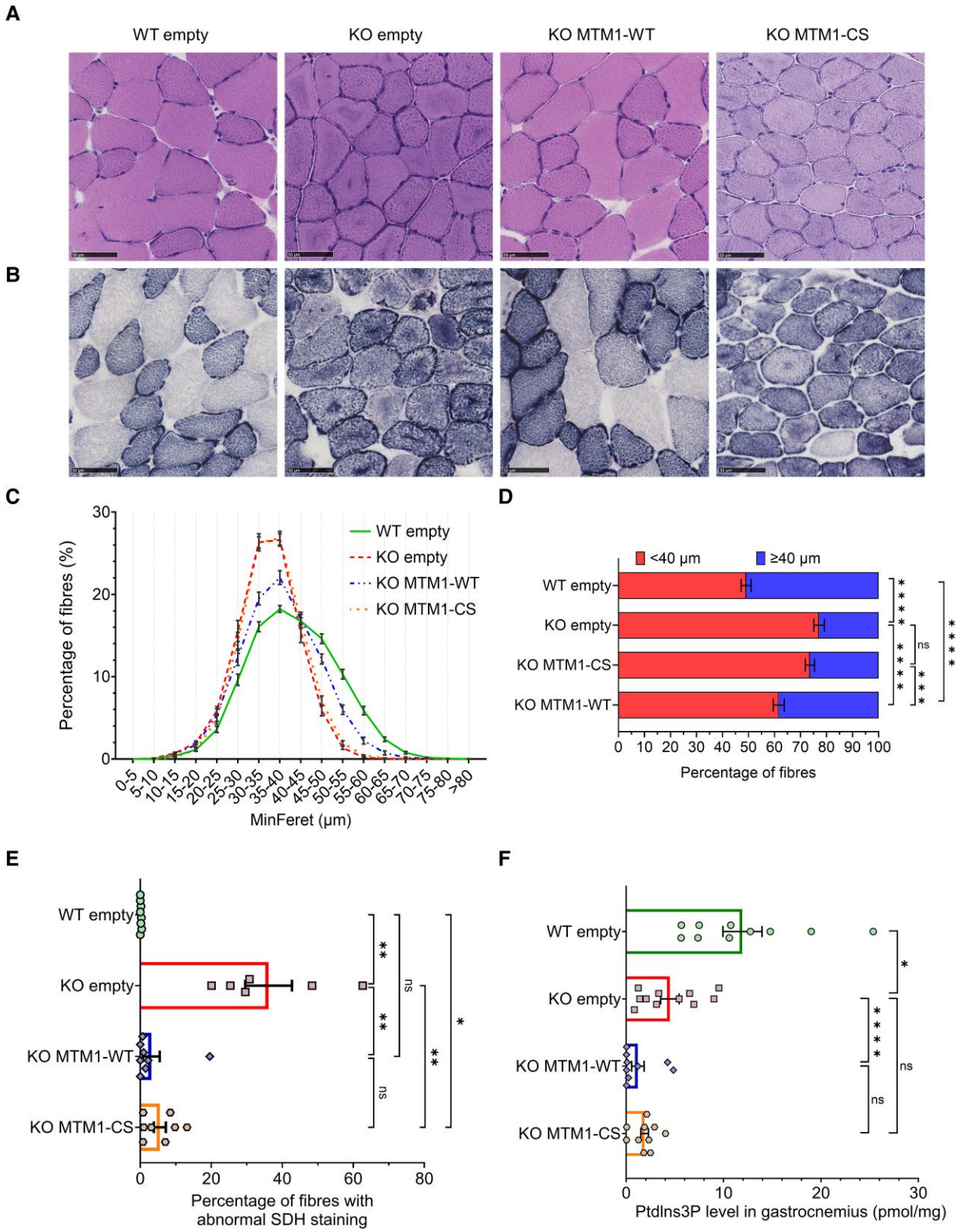

Figure 5 The phosphatase activity of MTM1 is required to improve myofibre size but not mitochondrial positioning. (**A**) Representative images of tibialis anterior (TA) stained by haematoxylin and eosin (**B**) and succinate dehydrogenase (SDH). Scale bar = 50 µm. (**C**) MinFeret diameter distribution of TA myofibres (**D**) and repartition between big (≥40 µm) and small (<40 µm) fibres. ($n \geq 11$) (**E**) Percentage of fibres presenting SDH accumulation in their centre ($n \geq 6$). (**F**) Phosphatidylinositol-3-phosphate (PtdIns3P) concentration in gastrocnemius muscle of 10-week-old mice ($n \geq 9$). One-way ANOVA followed by Fisher's LSD test, Kruskal-Wallis test followed by Dunn's test *$P < 0.05$, **$P < 0.01$, ***$P < 0.001$, ****$P < 0.0001$. KO = knockout; WT = wild-type.

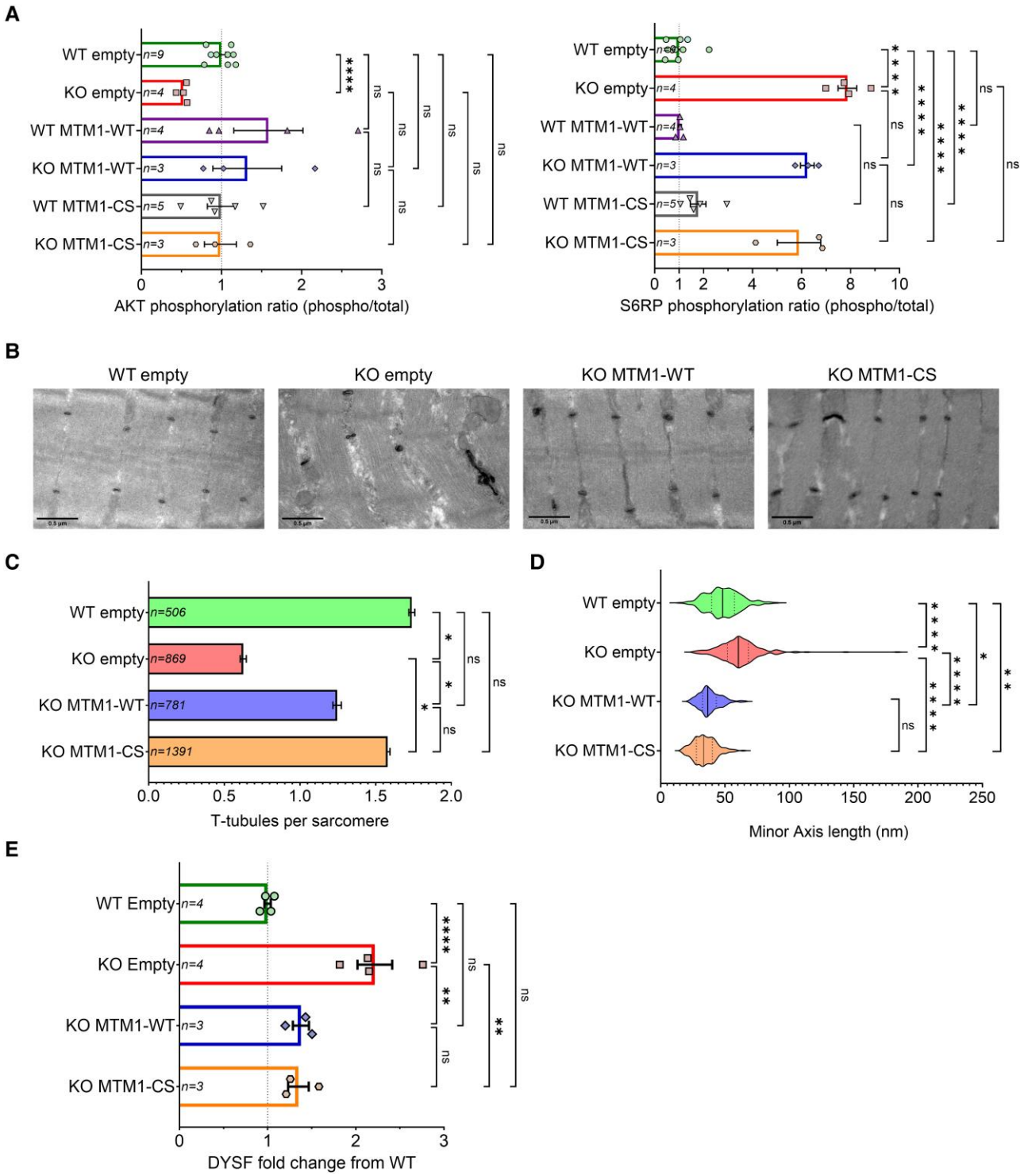

Figure 6 MTM1 overexpression rescues ultrastructure and improves mTOR pathway alterations. (**A**) Quantification of phosphorylation ratio by immunoblot analysis of AKT and S6RP total and phosphorylated forms, standardized to total proteins measured by ponceau S ($n \geq 3$). (**B**) Representative longitudinal electron microscopy pictures of tibialis anterior (TA) from 10-week-old mice with ferrocyanate staining. Scale bar = 500 nm. (**C**) Quantification of the number of T-tubules per sarcomere ($n = 2$, $n \geq 175$). (**D**) Measurement of the minor axis width of T-tubules ($n \geq 253$). (**E**) Immunoblot quantification of DYSF protein expression standardized to total proteins measured by ponceau S staining ($n \geq 3$). One-way ANOVA followed by Fisher's LSD test, unpaired *t*-test with Welch's correction, nested one-way ANOVA followed by Fisher's LSD test, Kruskal-Wallis test followed by Dunn's test. $^{*}P < 0.05$, $^{**}P < 0.01$, $^{****}P < 0.0001$. KO = knockout; WT = wild-type.

mice, DYSF and CAV3 levels were investigated. Both DYSF and CAV3 are increased in the *Bin1*$^{mck-/-}$ muscle, validating a defect in the regulation of T-tubule organization (Fig. 6E and Supplementary Fig. 8B and C). Concordantly, both MTM1-WT and MTM1-CS normalized DYSF levels and to a lesser extent CAV3 levels. Moreover, exogenous overexpression of MTM1 in wild-type muscles did not impact DYSF and CAV3 protein levels (Supplementary Fig. 9A and B), supporting that there is no direct regulation between MTM1 and DYSF/CAV3, and that DYSF/CAV3 levels reflect a compensatory effect due to T-tubules defect in the *Bin1* KO muscles. Taken together with the above data, the improvement of T-tubule ultrastructure correlates with the amelioration of motor and force function and is not dependent on the enzymatic activity of MTM1.

Partial reversion of the BIN1-CNM established phenotypes with late MTM1 expression

As shown in the data above, systemic expression of MTM1 from P1 prevented the development of the disease in the *Bin1*$^{mck-/-}$ mouse. Since patients can be affected early in life, we aimed to test a different protocol to revert an established phenotype by injecting the TA muscle at 8 weeks with AAV-MTM1-WT. The window of treatment was from 8 to 12 weeks. The total leg strength of *Bin1*$^{mck-/-}$ mice measured by a force transducer with foot plate was affected before 8 weeks and MTM1-WT expression ameliorated this parameter 3 weeks after injection; comparison of the AAV-MTM1-WT treated leg versus the AAV-empty injected contralateral leg of the same animal confirmed this effect (Fig. 7A and B). In addition, the TA muscle atrophy of *Bin1*$^{mck-/-}$ mice was ameliorated with AAV-MTM1-WT (Fig. 7C). While the total leg strength was improved, there was no noticeable rescue of the isolated TA muscle force after 4 weeks of treatment (Fig. 7D and E). We verified that muscles injected with AAV-MTM1-WT overexpressed the MTM1 protein (Supplementary Fig. 10A and B). Upon histological analysis, MTM1-WT expression was found to increase fibre size and improve mitochondria position in *Bin1*$^{mck-/-}$ muscle (Fig. 8A–C). At the ultrastructural level, we saw a general improvement of myofibre ultrastructure and notably a correction of the number of T-tubules per sarcomere (Fig. 8D-E). In conclusion, late intramuscular expression of MTM1 partially reverts leg weakness, muscle and myofibre atrophy, and the intracellular organization in the *Bin1*$^{mck-/-}$ mice after 4 weeks of treatment.

Discussion

Here, we aimed to validate a novel therapeutic approach for autosomal CNM in mice. We demonstrated that MTM1 exogenous overexpression strongly improved motor function, muscle force, the CNM histopathology and myofibre size and organization specifically in the *BIN1*-CNM mouse model. The lipid phosphatase activity was essential for the rescue of muscle atrophy and myofibre hypotrophy but dispensable for the rescue of myofibre disorganization including organelle misposition and T-tubule defects (Supplementary Table 1). Furthermore, the phenotypic rescue was accompanied by amelioration of the alterations in the AKT pathway. Early systemic MTM1 overexpression prevented the development of the CNM pathology in *Bin1*$^{mck-/-}$ mice, while late intramuscular MTM1 expression partially reverted the established phenotypes after only 4 weeks of treatment.

The fact that overexpression of MTM1 rescues the CNM phenotypes linked to BIN1 loss supports that these two proteins act synergistically to regulate a common function necessary for normal muscle physiology. Indeed, loss-of-function of either BIN1 or MTM1 causes CNM in humans and several mammals including mice and dogs.[3,14,31-33] Moreover, upregulating BIN1 rescued the *MTM1*-CNM form of the *Mtm1*$^{-/y}$ mouse,[34] and conversely, we show here upregulation of MTM1 rescues the *BIN1*-CNM form in *Bin1*$^{mck-/-}$ mice. In addition, MTM1 and BIN1 can interact and are part of the same complex in skeletal muscle.[13] We hypothesize overexpression of either MTM1 or BIN1 in CNM rescues the cellular function of the MTM1-BIN1 complex. Based on our data, this MTM1-BIN1 complex appears important for muscle hypertrophy, the intracellular organization of myofibres, and T-tubule ultrastructure. Indeed, the different genetic forms of CNM display muscle atrophy, organelles misposition and T-tubule defects.[3,35]

The rescue of the motor function and muscle force could rely on the hypertrophic effect of MTM1 expression specifically in the *Bin1*$^{mck-/-}$ mouse, and also on the amelioration of myofibre intracellular organization and T-tubule morphology. Noteworthy, the levels of two main regulators of T-tubule biogenesis and maintenance, DYSF and CAV3, are altered in the disease condition and rescued or partially rescued, respectively, upon MTM1 expression. Moreover, BIN1 is also a main regulator of T-tubule biogenesis and maintenance.[15,17]

The present data also revealed that the phosphatase activity is essential for the hypertrophic effect of MTM1 in the *Bin1*$^{mck-/-}$ mouse, but dispensable for the amelioration of T-tubule organization (Supplementary Table 1). The phosphatase-independent role of MTM1 in muscle should thus rely on protein-protein interaction, such as with BIN1 for T-tubule organization or desmin for mitochondria positioning.[13,36] Overall, the therapeutic effect of MTM1 in the *BIN1*-CNM model relies on the modulation of different complementary pathways regulating muscle mass and contraction.

Systemic MTM1 overexpression is efficient to prevent the development of the different motor and histological phenotypes in the *Bin1*$^{mck-/-}$ mouse when injected in the neonatal period. Thus, this strategy could be efficient to prevent the progression of general motor defects in patients. As a step toward clinical application, we also tested if AAV-MTM1 injection in affected adult mice could revert established phenotypes and found it ameliorated muscle strength, muscle atrophy and histopathology. Overall, this novel therapeutic strategy would then be applicable to a wide range of *BIN1*-CNM patients of different ages and at different stages of disease development.

Noteworthy, AAV-MTM1 was previously validated as a therapy in *MTM1*-CNM murine and canine models and more recently a clinical trial in young *MTM1*-CNM patients showed a significant improvement of motor and respiratory functions (ASPIRO; NCT03199469).[21] While our present data reveal that AAV-MTM1 injection efficiently rescued *BIN1*-CNM, they showed no effect on *DNM2*-CNM under the conditions tested. In conclusion, we show here that MTM1 exogenous expression is a common therapeutic strategy for different genetic forms of CNM (linked to MTM1 and BIN1 mutations), but not for the *DNM2*-CNM.

Of note, we used AAV serotype 9, which is used in clinic and as the basis of Zolgensma® (Novartis), a product efficiently preventing spinal muscular atrophy.[37] Concerning CNM, there is no clinical trial planned yet for *BIN1*-CNM. There are two gene modulation strategies tested in patients with other forms: AAV-MTM1 for *MTM1*-CNM patients exclusively (ASPIRO; NCT03199469) and *DNM2* antisense oligonucleotides for *MTM1*- and *DNM2*-CNM (UNITE-CNM; NCT04033159). Both trials are currently stopped due to adverse effects including hepatic toxicity.[38] In particular,

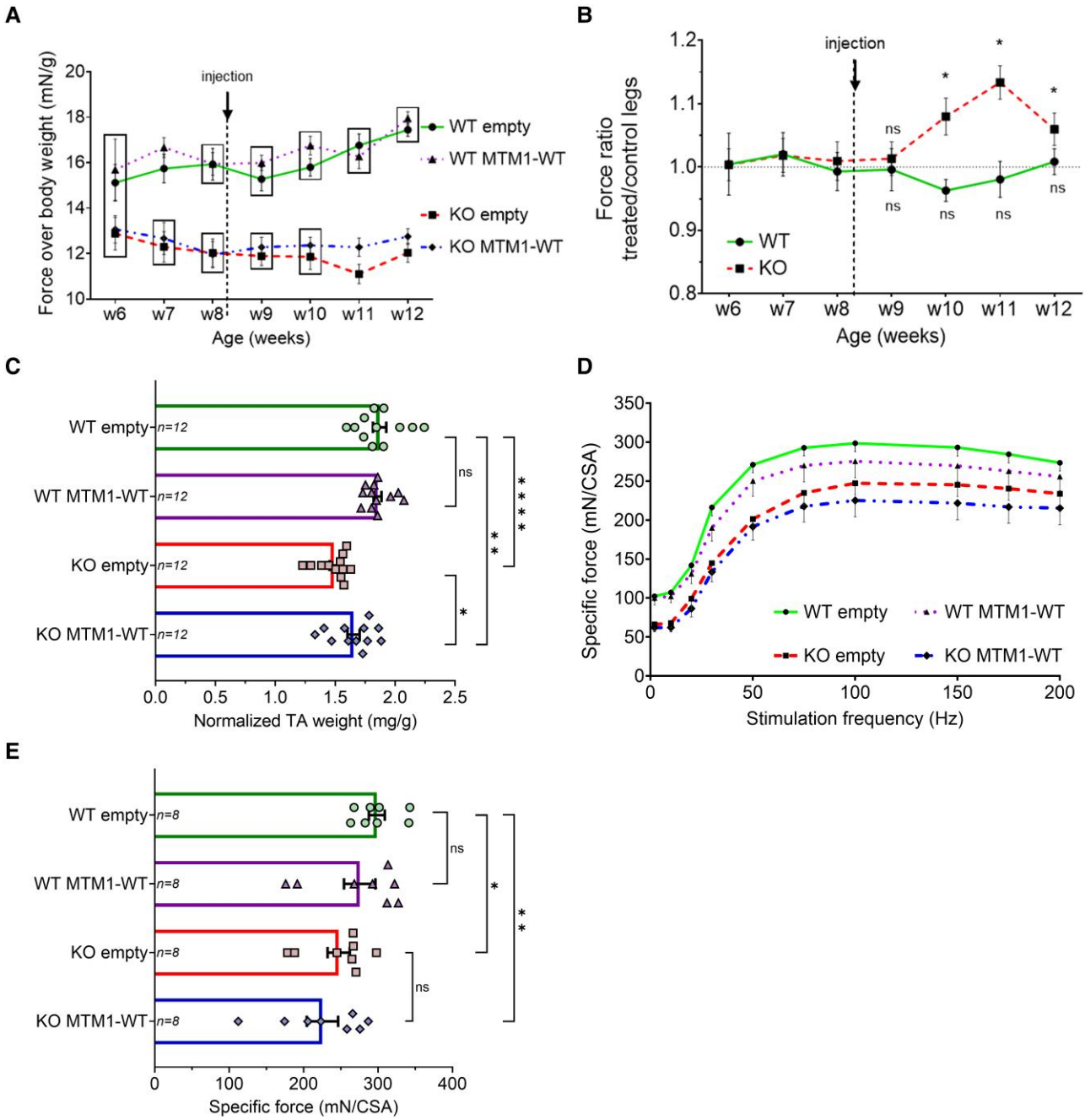

Figure 7 Late MTM1 overexpression improves muscle force and atrophy in adult *Bin1* KO animals. (**A**) *In vivo* maximal muscle force of the leg measured at 100 Hz. The boxes show groups with non-significant (ns) differences between treated (AAV-MTM1-WT) versus untreated (AAV-empty) contralateral legs. The dashed line indicates the time of injection ($n \geq 5$). (**B**) Force ratio between contralateral legs, evaluated against a hypothetical mean of 1 ($n \geq 5$). (**C**) Tibialis anterior (TA) muscle weight normalized to body weight at 12 weeks of age ($n = 12$). (**D**) *In situ* specific force measurement from TA muscles stimulated at different frequencies (**E**) and specific maximal muscle force measured at 100 Hz ($n = 8$). Multiple ratio paired *t*-test, multiple ratio unpaired *t*-test, one sample *t*-test, unpaired *t*-test with Welch's correction, unpaired *t*-test, $^{*}P < 0.05$, $^{**}P < 0.01$, $^{****}P < 0.0001$. KO = knockout; WT = wild-type.

AAV-MTM1 injection in *MTM1*-CNM patients exacerbated pre-existing hepatic defects and promoted intrahepatic cholestasis leading to liver failure and death in four patients.[38-40] Of note, *BIN1*-CNM patients were never reported to have any hepatic defects, unlike MTM1-CNM patients. Moreover, AAV-MTM1 administrated to MTM1-CNM patients showed amelioration of motor and respiratory function in several patients. Thus AAV-MTM1 could be beneficial for the motor function of *BIN1*-CNM patients without strong hepatic adverse effects. However, to further optimize the therapeutic approach, novel strategies should be explored to reduce the systemic dose of AAV. This could involve the use of novel myotropic capsids or tissue-specific promoters, as well as investigating intravenous delivery methods.[41-43] Such approaches have the potential to improve the safety profile and increase the feasibility of AAV-MTM1 treatment in BIN1-CNM patients. Developing an entirely new gene therapy product, such as

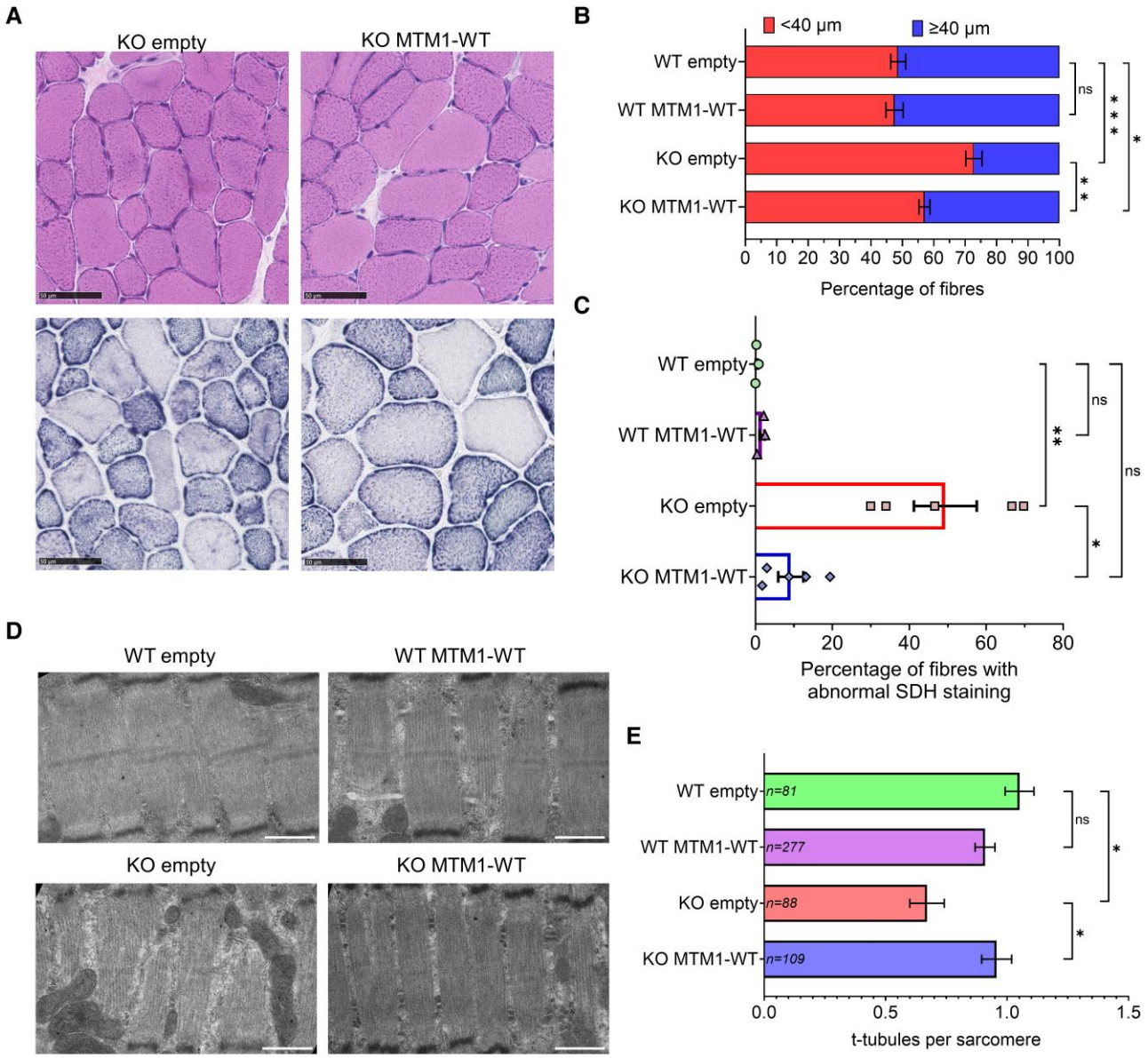

Figure 8 Late MTM1 overexpression ameliorates histological hallmarks of *Bin1* KO mice. (**A**) Representative images of the two contralateral tibialis anterior (TA) muscles from the same animal stained by haematoxylin and eosin and succinate dehydrogenase (SDH). Scale bar = 50 µm. (**B**) MinFeret diameter repartition of TA fibres between large (≥40 µm) and small (<40 µm) categories ($n \geq 5$). (**C**) Percentage of fibres presenting SDH accumulation in their centre ($n \geq 3$). (**D**) Representative longitudinal electron microscopy pictures of contralateral TA from 12-week-old mice. Scale bar = 500 nm. (**E**) Quantification of the number of T-tubules per sarcomere ($N = 3$, $n \geq 24$). Ratio paired *t*-test, unpaired *t*-test with Welch's correction, nested one-way ANOVA followed by Fisher's LSD test, $^{*}P < 0.05$, $^{**}P < 0.01$, $^{***}P < 0.001$. KO = knockout; WT = wild-type.

AAV-BIN1, would require additional time and resources that could be avoided by extending the use of AAV-MTM1 to BIN1 patients. Overall, our present data support the inclusion of *BIN1*-CNM patients in an AAV-MTM1 clinical trial.

Data availability

The authors confirm that the data supporting the findings of this study are available within the article and its Supplementary material.

Acknowledgements

We thank Valentina Maria Lionello, Xènia Massana Muñoz, Alix Simon, Christine Kretz, Marco Dalla Vecchio, Hugues Jacobs and Bertrand Vernay for their help with experiments and discussion; the photonic and electron microscopy, the histology, and the animal house platforms of IGBMC-ICS. We also thank Pascale Koebel and the molecular biology and virus service for the AAVs production.

Funding

This work of the Interdisciplinary Thematic Institute IMCBio, as part of the ITI 2021-2028 program of the University of Strasbourg, CNRS, and Inserm, was supported by Agence Nationale de la Recherche through the following programms: IdEx Unistra (ANR-10-IDEX-0002), SFRI-STRAT'US (ANR 20-SFRI-0012) and EUR IMCBio (ANR-17-EURE-0023) under the framework of the French Investments for the Future Program. This work was also supported

by Fondation pour la Recherche Médicale (EQU201903007992) and AFM-Téléthon (22734). Q.G. was supported by Fondation pour la Recherche Médicale (FDT202204015039).

Competing interests

J.L. is a co-founder of Dynacure.

Supplementary material

Supplementary material is available at *Brain* online.

References

1. Jungbluth H, Wallgren-Pettersson C, Laporte J. Centronuclear (myotubular) myopathy. *Orphanet J Rare Dis*. 2008;3:26.
2. Romero NB. Centronuclear myopathies: A widening concept. *Neuromuscul Disord*. 2010;20:223-228.
3. Gómez-Oca R, Cowling BS, Laporte J. Common pathogenic mechanisms in centronuclear and myotubular myopathies and latest treatment advances. *Int J Mol Sci*. 2021;22:11377.
4. Rossi D, Catallo MR, Pierantozzi E, Sorrentino V. Mutations in proteins involved in E-C coupling and SOCE and congenital myopathies. *J Gen Physiol*. 2022;154:e202213115.
5. Raess MA, Friant S, Cowling BS, Laporte J. WANTED - Dead or alive: Myotubularins, a large disease-associated protein family. *Adv Biol Regul*. 2017;63:49-58.
6. Hohendahl A, Roux A, Galli V. Structural insights into the centronuclear myopathy-associated functions of BIN1 and dynamin 2. *J Struct Biol*. 2016;196:37-47.
7. Antonny B, Burd C, De Camilli P, *et al*. Membrane fission by dynamin: What we know and what we need to know. *EMBO J*. 2016; 35:2270-2284.
8. Simunovic M, Evergren E, Callan-Jones A, Bassereau P. Curving cells inside and out: Roles of BAR domain proteins in membrane shaping and its cellular implications. *Annu Rev Cell Dev Biol*. 2019;35:111-129.
9. Towler MC, Kaufman SJ, Brodsky FM. Membrane traffic in skeletal muscle. *Traffic*. 2004;5:129-139.
10. Flucher BE, Takekura H, Franzini-Armstrong C. Development of the excitation-contraction coupling apparatus in skeletal muscle: Association of sarcoplasmic reticulum and transverse tubules with myofibrils. *Dev Biol*. 1993;160:135-147.
11. Rebbeck RT, Karunasekara Y, Board PG, Beard NA, Casarotto MG, Dulhunty AF. Skeletal muscle excitation-contraction coupling: Who are the dancing partners? *Int J Biochem Cell Biol*. 2014; 48:28-38.
12. Fujise K, Noguchi S, Takeda T. Centronuclear myopathy caused by defective membrane remodelling of dynamin 2 and BIN1 variants. *Int J Mol Sci*. 2022;23:6274.
13. Royer B, Hnia K, Gavriilidis C, Tronchère H, Tosch V, Laporte J. The myotubularin-amphiphysin 2 complex in membrane tubulation and centronuclear myopathies. *EMBO Rep*. 2013;14: 907-915.
14. Nicot AS, Toussaint A, Tosch V, *et al*. Mutations in amphiphysin 2 (BIN1) disrupt interaction with dynamin 2 and cause autosomal recessive centronuclear myopathy. *Nat Genet*. 2007;39: 1134-1139.
15. Lee E, Marcucci M, Daniell L, *et al*. Amphiphysin 2 (Bin1) and T-tubule biogenesis in muscle. *Science*. 2002;297:1193-1196.
16. Chin YH, Lee A, Kan HW, *et al*. Dynamin-2 mutations associated with centronuclear myopathy are hypermorphic and lead to T-tubule fragmentation. *Hum Mol Genet*. 2015;24: 5542-5554.
17. Razzaq A, Robinson IM, McMahon HT, *et al*. Amphiphysin is necessary for organization of the excitation-contraction coupling machinery of muscles, but not for synaptic vesicle endocytosis in Drosophila. *Genes Dev*. 2001;15:2967-2979.
18. Al-Qusairi L, Weiss N, Toussaint A, *et al*. T-tubule disorganization and defective excitation-contraction coupling in muscle fibers lacking myotubularin lipid phosphatase. *Proc Natl Acad Sci U S A*. 2009;106:18763-18768.
19. Silva-Rojas R, Nattarayan V, Jaque-Fernandez F, *et al*. Mice with muscle-specific deletion of bin1 recapitulate centronuclear myopathy and acute downregulation of dynamin 2 improves their phenotypes. *Mol Ther*. 2022;30:868-880.
20. Muñoz XM, Kretz C, Silva-Rojas R, *et al*. Physiological impact and disease reversion for the severe form of centronuclear myopathy linked to dynamin. *JCI Insight*. 2020;5:e137899.
21. Childers MK, Joubert R, Poulard K, *et al*. Gene therapy prolongs survival and restores function in murine and canine models of myotubular myopathy. *Sci Transl Med*. 2014;6:220ra10.
22. Amoasii L, Bertazzi DL, Tronchere H, *et al*. Phosphatase-dead myotubularin ameliorates X-linked centronuclear myopathy phenotypes in mice. *PLoS Genet*. 2012;8:e1002965.
23. Cowling BS, Prokic I, Tasfaout H, *et al*. Amphiphysin (BIN1) negatively regulates dynamin 2 for normal muscle maturation. *J Clin Invest*. 2017;127:4477-4487.
24. Brüning JC, Michael MD, Winnay JN, *et al*. A muscle-specific insulin receptor knockout exhibits features of the metabolic syndrome of NIDDM without altering glucose tolerance. *Mol Cell*. 1998;2:559-569.
25. Stringer C, Wang T, Michaelos M, Pachitariu M. Cellpose: A generalist algorithm for cellular segmentation. *Nat Methods*. 2021; 18:100-106.
26. Bankhead P, Loughrey MB, Fernandez JA, *et al*. Qupath: Open source software for digital pathology image analysis. *Sci Rep*. 2017;7:16878.
27. Schindelin J, Arganda-Carreras I, Frise E, *et al*. Fiji: An open-source platform for biological-image analysis. *Nat Methods*. 2012;9:676-682.
28. Böhm J, Biancalana V, Dechene ET, *et al*. Mutation spectrum in the large GTPase dynamin 2, and genotype-phenotype correlation in autosomal dominant centronuclear myopathy. *Hum Mutat*. 2012;33:949-959.
29. Sartori R, Romanello V, Sandri M. Mechanisms of muscle atrophy and hypertrophy: Implications in health and disease. *Nat Commun*. 2021;12:330.
30. Al-Qusairi L, Laporte J. T-tubule biogenesis and triad formation in skeletal muscle and implication in human diseases. *Skelet Muscle*. 2011;1:26.
31. Laporte J, Hu LJ, Kretz C, *et al*. A gene mutated in X-linked myotubular myopathy defines a new putative tyrosine phosphatase family conserved in yeast. *Nat Genet*. 1996;13:175-182.
32. Bohm J, Vasli N, Maurer M, *et al*. Altered splicing of the BIN1 muscle-specific exon in humans and dogs with highly progressive centronuclear myopathy. *PLoS Genet*. 2013;9:e1003430.
33. Beggs AH, Böhm J, Snead E, *et al*. MTM1 Mutation associated with X-linked myotubular myopathy in labrador retrievers. *Proc Natl Acad Sci U S A*. 2010;107:14697-14702.
34. Lionello VM, Nicot AS, Sartori M, *et al*. Amphiphysin 2 modulation rescues myotubular myopathy and prevents focal adhesion defects in mice. *Sci Transl Med*. 2019;11:eaav1866.
35. Lawlor MW, Dowling JJ. X-linked myotubular myopathy. *Neuromuscul Disord*. 2021;31:1004-1012.
36. Hnia K, Tronchere H, Tomczak KK, *et al*. Myotubularin controls desmin intermediate filament architecture and mitochondrial

dynamics in human and mouse skeletal muscle. *J Clin Invest*. 2011;121:70-85.
37. Mendell JR, Al-Zaidy S, Shell R, *et al*. Single-Dose gene-replacement therapy for spinal muscular atrophy. *N Engl J Med*. 2017;377:1713-1722.
38. Shieh PB, Bonnemann CG, Muller-Felber W, *et al*. Re: "Moving forward after two deaths in a gene therapy trial of myotubular myopathy" by Wilson and Flotte. *Hum Gene Ther*. 2020;31(15–16):787.
39. Molera C, Sarishvili T, Nascimento A, *et al*. Intrahepatic cholestasis is a clinically significant feature associated with natural history of X-linked myotubular myopathy (XLMTM): A case series and biopsy report. *J Neuromuscul Dis*. 2022;9:73-82.
40. D'Amico A, Longo A, Fattori F, *et al*. Hepatobiliary disease in XLMTM: A common comorbidity with potential impact on treatment strategies. *Orphanet J Rare Dis*. 2021;16:425.
41. Tabebordbar M, Lagerborg KA, Stanton A, *et al*. Directed evolution of a family of AAV capsid variants enabling potent muscle-directed gene delivery across species. *Cell*. 2021;184:4919-4938.e22.
42. Weinmann J, Weis S, Sippel J, *et al*. Identification of a myotropic AAV by massively parallel in vivo evaluation of barcoded capsid variants. *Nat Commun*. 2020;11:5432.
43. Skopenkova VV, Egorova TV, Bardina MV. Muscle-Specific promoters for gene therapy. *Acta Naturae*. 2021;13:47-58.